Journal of Physics: Conference Series

High-T_c micro and nano-constrictions modeling: hot spot approach for DC characteristics and HEB THz mixer performance

To cite this article: Romain G Ladret *et al* 2014 *J. Phys.: Conf. Ser.* **507** 042020

High-T_C micro and nano-constrictions modeling: hot spot approach for DC characteristics and HEB THz mixer performance

Romain G Ladret, Annick F Dégardin and Alain J Kreisler[1]
SUPÉLEC LGEP; CNRS UMR 8507; UPMC Univ Paris 06; Univ Paris-Sud 11;
11 rue Joliot-Curie, 91192 GIF SUR YVETTE Cedex, France

E-mail: alain.kreisler@supelec.fr

Abstract. High-T_C hot electron bolometers (HEB) are promising THz mixers due to their expected wide bandwidth, large mixing gain, and low intrinsic noise. We have simulated the characteristics of YBaCuO HEBs with a hot spot model usually dedicated to low-T_C phonon cooled devices. With respect to e.g., NbN, the high-T_C specificities are mainly arising from the large values of YBaCuO phonon thermal conductivity, and the film to MgO substrate phonon escape time. The consequent effects on the electron temperature profiles along the YBaCuO constriction and the current voltage DC characteristics are considered. The conversion gain G and noise temperature T_N were computed for two constriction dimensions. For a 100 nm long × 100 nm wide × 10 nm thick constriction at 9 microwatt local oscillator (LO) power, the expected double sideband (DSB) T_N = 1520 K (G = –13.7 dB). For a larger (but more realistic according to YBaCuO aging effects) 400 nm long × 400 nm wide × 35 nm thick constriction, minimum T_N = 1210 K DSB at 35 microwatt LO power (G = –13.1 dB).

1. Introduction

During the past decade, superconducting hot electron bolometers (HEB) have been the object of unceasing progress. The performances achieved by low-T_C devices are at a very high level in terms of heterodyne mixing in the THz. For example, double sideband (DSB) noise temperatures T_N = 950 K [1] and 600 K [2] at 2.5 THz were reported for NbN HEBs. Efforts on high-T_C HEBs ($YBa_2Cu_3O_{7-\delta}$ - YBCO) have been, however, more limited, with few published results from microwave to THz frequencies [3-6]. Indeed, YBCO HEB technology has proven difficult due to the chemical reactivity and the aging effects of YBCO ultrathin films. Such films are required to achieve sensitive HEBs, but a sharp increase in conversion losses results from aging [7,8]. However, predicted performance was particularly encouraging, with T_N = 2000 K (single sideband – SSB) at P_{LO} = 11 μW local oscillator (LO) power for an YBCO constriction of 10 nm thickness and 100×100 nm^2 transverse dimensions [9]. This first model was based on the "0-D" point bolometer approach, which describes the system in terms of thermal reservoirs only, namely the electrons of the superconducting film at temperature T_e and the phonons of the film at temperature $T_p < T_e$. The electron - phonon interaction time τ_{ep} drives the HEB transient response or its instantaneous bandwidth as a mixer. With τ_{ep} = 1-2 ps, the YBCO HEB gives the hope of a bandwidth close to 100 GHz (but so far unobserved), whereas NbN exhibits

[1] To whom any correspondence should be addressed.

$\tau_{ep} \approx 20$ ps. Moreover, the "1-D" hot spot model, which takes into account the spatial dependence of T_e along the superconducting constriction, was implemented for low-T_C HEBs [10]. Our motivation was to apply this model to YBCO, while taking the high-T_C specificities into account, which are mainly due to the large phonon thermal conductivity and the long film to substrate phonon escape time τ_{esc}.

2. HEB geometry and thermal equations

The main constituents of an YBCO-based HEB are shown in figure 1. The superconducting ultrathin film is deposited on an MgO substrate (with lattice matching buffer layer). The YBCO constriction is coupled to the rf radiation by means of a planar metal antenna.

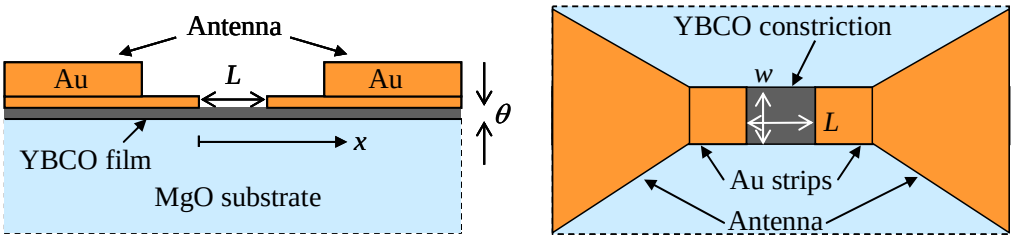

Figure 1. HEB schematics (not to scale) depicting the YBCO constriction connected to the arms of a planar antenna. Left: cross-section; right: top view. The constriction dimensions are: length L, width w, and thickness θ. The hot-spot model coordinate x is parallel to L.

The thermal exchange in the device is governed by the heat equations pertaining to the electrons (1) and the phonons (2) of the YBCO film, bearing indices e and p, respectively:

$$V_c\kappa_e\left(T_{ec}\right)\frac{\delta^2 T_e}{\delta x^2} - V_c C_e\left(T_{ec}\right)\frac{\delta T_e}{\delta t} = \frac{V_c C_e}{n\tau_{ep}T_{ec}^{n-1}}\left(T_e^n - T_p^n\right) - P_{LO} - P_J \ , \tag{1}$$

$$V_c\kappa_p\left(T_{pc}\right)\frac{\delta^2 T_p}{\delta x^2} - V_c C_p\left(T_{pc}\right)\frac{\delta T_p}{\delta t} = \frac{V_c C_p}{m\tau_{esc}T_{pc}^{m-1}}\left(T_p^m - T_0^m\right) - \frac{V_c C_e}{n\tau_{ep}T_{ec}^{n-1}}\left(T_e^n - T_p^n\right) \ , \tag{2}$$

where the only spatial coordinate x is along the length of the constriction (figure 1), which is anchored to its ends at the thermostat temperature T_0; i.e., $x \in [0,L]$, with $T_e(0) = T_e(L) = T_0$. V_c is the constriction volume; $\kappa_{e,p}$ and $C_{e,p}$ are the thermal conductivities and volumic specific heats, respectively (evaluated at the assumed constant temperatures T_{ec}, T_{pc}). The power source terms are P_{LO} and the DC bias Joule power P_J. Equations (1) and (2) are depicting a phonon cooled device, because cooling by the electron diffusion to the metal contacts can be neglected in YBCO [9].

3. Solving hypotheses and DC characteristics

Apart from general simplifying assumptions (YBCO material homogeneity, uniform current density in the constriction section, temperature independent thermal conductivities and specific heats, no LO losses), other hypotheses are more specific.

i) As the phonon thermal conductivity is one order of magnitude larger for YBCO at ~ 80 K than for NbN at ~ 10 K, the second order derivative in (2) cannot be neglected as in [10].

ii) Due to film/substrate interface nature (lattice mismatch and/or buffer layer), the phonon escape time is much longer in YBCO/MgO; i.e., τ_{esc} (ps) $\approx 75\times\theta$ (nm) [11] ($\approx 13\times\theta$ in NbN/Si [10]).

iii) The thermal exchange exponents are $m = n = 3$ for YBCO ($m = 4$ and $n = 3.6$ for NbN) [9,10].

The numerical values for the various parameters are gathered in table 1. Two devices have been simulated; Device A represents a constriction close to the limits of achievable e-beam lithography (same dimensions as in [9]) and Device B represents our currently achievable dimensions [8].

Table 1. Simulated device parameter values.

	L nm	W nm	θ nm	τ_{ep} ps	τ_{esc} ps	κ_e $Wm^{-1}K^{-1}$	κ_p $Wm^{-1}K^{-1}$	T_C [a] K	ΔT [b] K	J_C [c] Acm^{-2}	ρ [d] Ωcm	T_0 K
Dev. A	100	100	10	1.0	0.75	1	10	85	1.2	2×10^6	3×10^{-4}	60
Dev. B	400	400	35	1.7	2.6	1	10	89	1.2	2×10^6	3×10^{-4}	70

[a]At mid-transition [b]Transition width [c]At 77 K [d]Normal state resistivity at ≈ 100 K

Solving was performed in steady-state conditions (time derivatives omitted) using the MATLAB® ordinary differential equations toolbox. Temperature profiles for Device A are shown in figure 2 and DC current-voltage plots are shown in figure 3 for both devices. The hot electron effect ($T_e > T_p$) is clearly visible in figure 2a, as well as the hot spot central region ($T_e > T_C$ at I = 188 μA). Negative resistance is observed for device A at low LO levels (figure 3a), whereas it is not visible for device B (figure 3b) seemingly due to the damping effect of the larger thermal resistance associated to the longer τ_{esc}. The effect of neglecting the phonon diffusion along the constriction (second order derivative term in (2) suppressed) shows a much larger electron heating effect (figure 2b) and no negative resistance (figure 2b, inset), as discussed in [12].

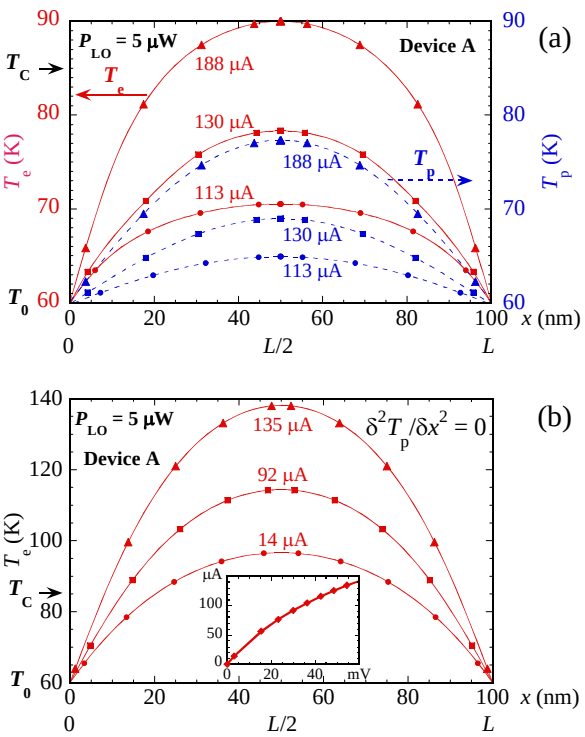

Figure 2. Temperature profiles for device A at various DC bias current values. (a): T_e and T_p plots. (b): T_e plots with second order T_p term neglected (inset: corresponding DC *I-V* plot).

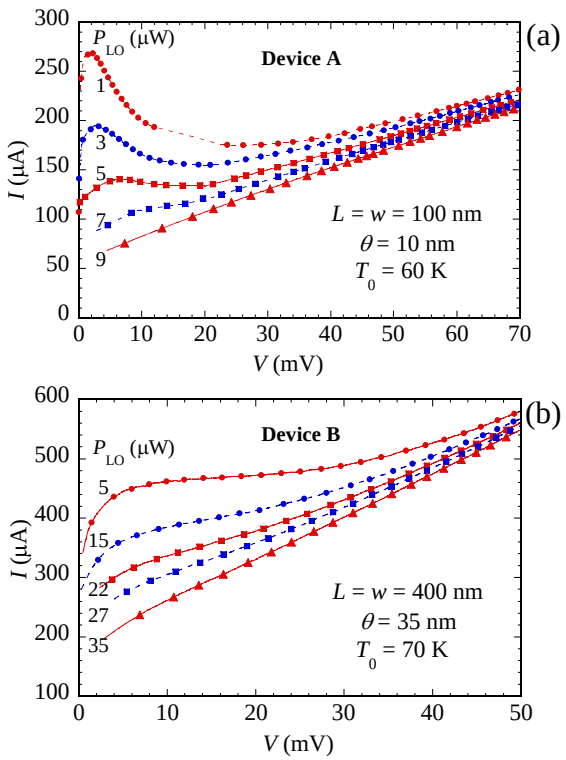

Figure 3. DC *I-V* plots at various LO power values, for device A (a) and device B (b). The sign of dI/dV is sensitive to the second order T_p term (P_{LO} = 5 μW in (a) and inset in figure 2b).

4. HEB mixer performances

The conversion gain G and noise temperature T_N were extracted from the large signal analysis, as performed in [10] for NbN devices. G is defined as the ratio between the power dissipated into the device loading resistance (50 Ω) and the signal power absorbed by the device. It contains both the DC and LO power efficiencies. T_N is the sum of the DSB temperatures due to the thermal fluctuations and Johnson noise. The most significant performances are gathered in table 2.

Table 2. Minimum DSB noise temperature and maximum conversion gain for both YBCO devices.

	Device A			Device B		
P_{LO} (μW)	1	5	9	5	15	35
T_{Nmin} (K)	6200	2000	1520	4000	1730	1210
V (mV) / I (μA)[a]	24 / 175	19.5 / 135	10.5 / 83	19 / 470	16.5 / 400	9.5 / 260
G (dB)[a]	–19	–14.9	–13.7	–16.6	–13.9	–13.1
G_{max} (dB)	–2	–6	–13.4	–15.6	–12.2	–12.6
V (mV) / I (μA)[b]	3.6 / 255	2.8 / 130	6.5 / 74	12.5 / 465	8 / 375	7 / 235
T_N (K)[b]	19800	5700	1620	5150	2250	1350

[a]For T_{Nmin}: DC bias point and associated gain [b]For G_{max}: DC bias point and associated noise temperature

For device A, P_{LO} = 9 μW allows to achieve T_{Nmin} = 1520 K DSB with G = –13.7 dB (close to G_{max} = –13.4 dB), whereas the point bolometer model provides $T_N \approx$ 1000 K (2000 K SSB) at P_{LO} = 11 μW [9]. High G values could be achieved at low P_{LO} levels, due to the negative resistance effect (figure 3a), but the noise dramatically increases. For device B, optimal performance is achieved at P_{LO} = 35 μW, with $T_N \approx$ 1200 to 1350 K and $G \approx$ –13 to –12.5 dB, respectively.

5. Conclusions

Starting from a hot spot model developed for NbN HEBs, we have revised the physical hypotheses to fully represent the YBCO specificities. Good mixer performance could be obtained with a device of reasonable dimensions, according to the YBCO sensitivity to technological process. Further improvements will concern the behavior at THz frequencies and the mixer bandwidth.

Acknowledgment

This work has been supported by the French National Research Agency (ANR) under grant # 2011-BS03-008-01.

References

[1] Baselmans J J A, Hajenius M, Gao J R, Klapwijk T M, de Korte P A J, Voronov B and Gol'tsman G N 2004 *Appl. Phys. Lett.* **84** 1958
[2] Tretyakov I, Ryabchun S, Finkel M, Maslennikova A, Kaurova N, Lobastova A, Voronov B and Gol'tsman G 2011 *Appl. Phys. Lett.* **98** 033507
[3] Li C-T, Deaver B S, Lee M, Weikle II R M, Rao R A and Eom C-B 1998 *Appl. Phys. Lett.* **73** 1727
[4] Harnack O, Il'in K S, Siegel M, Karasik B S, McGrath W R and De Lange G 2001 *Appl. Phys. Lett.* **79** 1906
[5] Gousev Y P, Semenov A D, Nebosis R S, Pechen E V, Varlashkin A V and Renk K F 1996 *Supercond. Sci. Technol.* **9** 779
[6] Cherednichenko S, Rönnung F, Gol'tsman G, Kollberg E and Winkler D 2000 *Proc. 11th Int. Symp. Space Terahertz Technology* www.nrao.edu/isstt/papers/2000517528.pdf
[7] Péroz Ch, Dégardin A F, Villégier J-C and Kreisler A J 2007 *IEEE Trans. Appl. Supercond.* **17** 637
[8] Aurino M, Kreisler A J, Türer I, Martinez A, Gensbittel A and Dégardin A F 2010 *J. Phys.: Conf. Ser.* **234** 042002
[9] Karasik B S, McGrath W R and Gaidis M C 1997 *J. Appl. Phys.* **81** 1581
[10] Khosropanah P, Merkel H, Yngvesson S, Adam A, Cherednichenko S, and Kollberg E 2000 *Proc. 11th Int. Symp. Space Terahertz Technology* 474-488
[11] Harrabi K, Ladan F-R, Vu Dinh Lam, Maneval J-P, Hamet J-F, Villégier J-C and Bland R W 2009 J. Low Temp. Phys. **157** 36
[12] Ladret R G, Dégardin A F and Kreisler A J 2013 *IEEE Trans. Appl. Supercond.* **23** 23003305